

An optical spectrum analyzer with quantum limited noise floor

M. Bishof, X. Zhang, M. J. Martin, and Jun Ye

JILA, National Institute of Standards and Technology and University of Colorado,
Department of Physics, University of Colorado, Boulder, CO 80309, USA.

(Dated: July 19, 2022)

Interactions between atoms and lasers provide the potential for unprecedented control of quantum states. Fulfilling this potential requires detailed knowledge of frequency noise in optical oscillators with state-of-the-art stability. We demonstrate a technique that precisely measures the noise spectrum of an ultra-stable laser using optical lattice-trapped ^{87}Sr atoms as a quantum projection noise-limited reference. We determine the laser noise spectrum from near DC to 100 Hz via the measured fluctuations in atomic excitation, guided by a simple and robust theory model. The noise spectrum yields a 26(4) mHz linewidth at a central frequency of 429 THz, corresponding to an optical Q of 1.6×10^{16} . This approach improves upon optical heterodyne beats between two similar laser systems by providing information unique to a single laser, and complements the traditionally used Allan deviation which evaluates laser performance at relatively long time scales. We use this technique to verify the reduction of resonant noise in our ultra-stable laser via feedback from an optical heterodyne beat. Finally, we show that knowledge of our laser's spectrum allows us to accurately predict the laser-limited stability for optical atomic clocks.

The utility of a precision frequency source is limited by its instabilities. For this reason, many methods to rigorously characterize these instabilities have been developed [1]. Ultra-stable lasers pose a unique challenge to characterizing frequency instabilities because, until now, measurements of their performance required an optical heterodyne beat between two or more lasers [2–7]. Single laser performance can be inferred from a three-cornered hat type measurement [8, 9], but valuable information about a laser's frequency noise power spectral density (PSD) [10] is limited in an optical beat by the less stable laser.

Optical lattice trapped ^{87}Sr atoms are uniquely suited for laser noise spectral analysis due to the ultra-narrow linewidth and field insensitivity of the 1S_0 ($|g\rangle$) to 3P_0 ($|e\rangle$) clock transition as well as the low quantum projection noise (QPN) one can achieve with ensembles of many atoms. To accomplish this, we adopt a technique similar to radio-frequency-based dynamical decoupling [11–14] to manipulate the frequency noise sensitivity of the ^{87}Sr optical clock transition. We demonstrate the ability to characterize the noise spectrum of an ultra-stable laser with fractional frequency stability at 1×10^{-16} . To guide and interpret our experimental measurements, we develop a simple and robust theoretical framework that combines concepts from the characterization of frequency instabilities [1] with a model for atomic sensitivity to frequency fluctuations [15–18]. We compare experimentally measured fluctuations in atomic population to our theory and accurately determine the PSD of our laser. As laser stability advances, we can continue to leverage the QPN-limited noise floor of this technique to analyze lasers with greater stability. At the same time, atoms could serve to stabilize lasers at the level of intrinsic atomic coherence [19, 20].

To model the frequency of our ultra-stable laser, we consider a fixed frequency with a small, time-dependent noise term: $\omega_L(t) = \omega_{L_0} + \delta\omega(t)$. The instantaneous phase of the laser is then given by $\phi_L(t) = \int_0^t dt' \omega_L(t') = \omega_{L_0}t + \int_0^t dt' \delta\omega(t') \equiv \omega_{L_0}t + \delta\phi(t)$. The resulting Hamiltonian for a

two level atom, with energy spacing $\hbar\omega_a$, driven by this laser is given by [21]

$$\frac{\hat{H}}{\hbar} = -\frac{\Omega(t)}{2} \begin{pmatrix} 0 & e^{i\delta\phi(t)} \\ e^{-i\delta\phi(t)} & 0 \end{pmatrix} - \frac{\bar{\Delta}}{2} \hat{\sigma}_z, \quad (1)$$

where $\bar{\Delta} \equiv \omega_{L_0} - \omega_a$, $\hat{\sigma}_z$ is a Pauli spin matrix, and $\Omega(t)$ is the Rabi frequency. The time dependence of $\Omega(t)$ relates to the chosen spectroscopy sequence. In the absence of other perturbations, the atom behaves as a filter, through which laser instabilities can be viewed. To calculate the output of our “atomic filter,” we will need to know the atom's impulse response. This quantity describes the atomic response to frequency deviations of the form $\delta\omega(t, t_0) = \Delta\phi \delta(t - t_0)$, where $\delta(t)$ is the Dirac delta function and $\Delta\phi$ is infinitesimally small. Using the definition of $\delta\phi(t)$ from above, we see that this is equivalent to considering an instantaneous step in $\delta\phi(t)$ at time t_0 . $\delta\phi(t)$ can also account for deliberate phase shifts of the laser which we implement during spectroscopy.

The measured quantity of our system is the population imbalance between $|g\rangle$ and $|e\rangle$. For a given atomic state $|\psi\rangle = a|g\rangle + b|e\rangle$, the population imbalance is defined as $\mathbb{P} \equiv bb^* - aa^*$. Keeping with the filter analogy, we can express \mathbb{P} as

$$\mathbb{P} = \mathbb{P}_0 + \int_{-\infty}^{\infty} dt r(t) \Delta(t), \quad (2)$$

where \mathbb{P}_0 is the initial imbalance, $\Delta(t) \equiv \bar{\Delta} + \delta\omega(t)$, and $r(t)$ is the impulse response [1], commonly referred to as the sensitivity function [16, 17]. The above equation defines $r(t)$ and then calculating the effect of frequency noise on \mathbb{P} reduces to calculating $r(t)$. Inserting the above form of $\delta\omega(t, t_0)$ into (2) and differentiating with respect to $\Delta\phi$, we get

$$\frac{\partial \mathbb{P}}{\partial \Delta\phi} \bigg|_{\Delta\phi=0} = \int_{-\infty}^{\infty} dt r(t) \delta(t - t_0) = r(t_0). \quad (3)$$

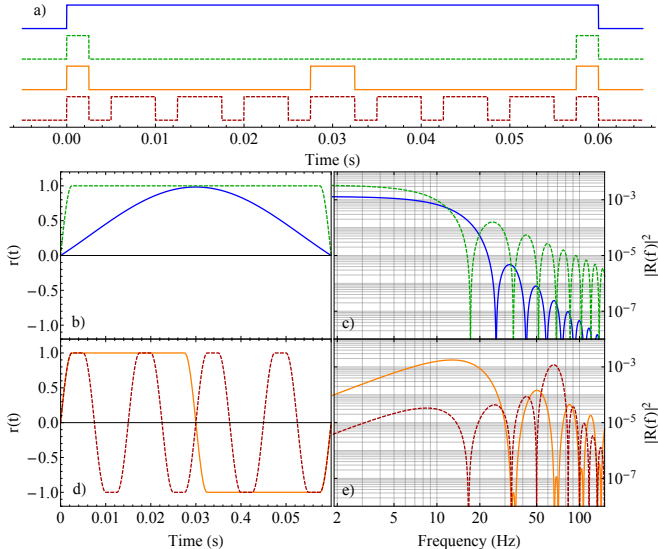


FIG. 1. (Color online) Schematic diagrams, $r(t)$, and $|R(f)|^2$ for different spectroscopy sequences. An example total spectroscopy time of 60 ms is shown. Throughout this work, blue(green) represents Rabi(Ramsey) spectroscopy and orange(red) represents 1-(7)-echo pulse spectroscopy. The schematic diagrams shown in (a) signify when $\Omega(t)$ is nonzero by their “high” value and signify free evolution ($\Omega(t) = 0$) with their “low” value. For Rabi spectroscopy, the nonzero value of Ω is selected such that the total pulse area of the spectroscopy pulse is π . For the other spectroscopy sequences, the nonzero value of Ω is always $\pi/(0.005)$ rad/s. The diagrams are offset in height for clarity. Plots of $|R(f)|^2$ in (c) and (e) are calculated from the corresponding $r(t)$ curves plotted in (b) and (d). Diagrams and functions related to modified Ramsey and 7-echo pulse spectroscopy are plotted with dashed lines for clarity.

We calculate \mathbb{P} using (1) for a particular spectroscopy sequence, $\Omega(t)$, and with an added phase step of $\Delta\phi$ occurring at time t_0 . Finally, $r(t)$ is calculated by allowing t_0 to vary throughout the spectroscopy sequence.

Eqn. (2) allows us to rigorously connect the observed fluctuations in \mathbb{P} to $\Delta(t)$. An essential quantity to consider is the variance of \mathbb{P} , $I^2 \equiv \langle \mathbb{P}^2 \rangle - \langle \mathbb{P} \rangle^2$, which can be expressed as [21]:

$$I^2 = (2\pi)^2 \int_0^\infty df S_\nu(f) |R(f)|^2. \quad (4)$$

Here, $R(f)$ is the Fourier transform of $r(t)$ and $S_\nu(f)$ is the single sided frequency noise PSD of the laser in units of Hz^2/Hz . Fig. 1 shows a schematic diagram for the spectroscopy sequences used in this work along with their corresponding sensitivity functions, $r(t)$ and $|R(f)|^2$, for a total spectroscopy time of 60 ms.

For Rabi and Ramsey spectroscopy, the theoretical value for I diverges since thermal noise, a fundamental limit to $S_\nu(f)$ at low frequency, has an f^{-1} character. For these measurements, we use the Allan Deviation [22] to characterize fluctuations in \mathbb{P} . In particular, we consider the two-sample Allan variance,

defined as

$$I_{(2)}^2 \equiv \frac{1}{2} \langle (\mathbb{P}_{i+1} - \mathbb{P}_i)^2 \rangle, \quad (5)$$

where the index, i , signifies the i th measurement of \mathbb{P} . In the treatment of multiple measurements we consider the sensitivity function as periodic with a period equal to the experimental cycle time, T_c . For this work, T_c is approximately 1 s plus the spectroscopy time. $I_{(2)}^2$ can also be expressed in terms of $S_\nu(f)$ in the following way [21]:

$$I_{(2)}^2 = (2\pi)^2 \int_0^\infty df S_\nu(f) 2 \sin^2(\pi f T_c) |R(f)|^2. \quad (6)$$

Although the theoretical value of $I_{(2)}$ remains finite for all data conditions, it does not properly account for coherent vibrational or electronic noise that exists on our laser at frequencies above 20 Hz. This noise is aliased onto our measurements and leads to regular, slow oscillations of the measured \mathbb{P} . Therefore, for echo pulse sequences we use I to characterize our measurements. The Rabi and Ramsey sequences do not suffer from aliasing of coherent noise since they do not have significant sensitivity to noise above 20 Hz for the spectroscopy times used here.

Our experimental setup follows that of our Sr clock [23, 24]. Between 2000 and 3000 ^{87}Sr atoms are cooled to about 2 μK in a one-dimensional optical lattice and nuclear spin polarized into the ground $^1S_0 m_F = 9/2$ state. The optical lattice is kept near the magic wavelength [25] for the $|g\rangle$ to $|e\rangle$ clock transition. Lattice-trapped atoms are excited with 698 nm light according to the spectroscopy sequences shown in Fig. 1(a). The clock light propagates along the strongly confined axis of the lattice so that it probes the atoms in the well-resolved sideband regime, free from Doppler and recoil effects. Finally, the numbers of atoms in $|g\rangle$ and $|e\rangle$ are measured to determine \mathbb{P} .

Using this setup, we have resolved 0.5 Hz spectral features [26, 27] and demonstrated the most stable optical clock [28]. These results are enabled by the ultra-stable laser that addresses the clock transition (hereafter termed “ α -laser”). The stability of the α -laser is at its thermal noise limit of 1×10^{-16} fractional frequency units for ~ 1 to 1000 s. We can look for strong noise features at higher frequencies in the α -laser’s $S_\nu(f)$ using an optical beat with a second laser (hereafter termed “ β -laser”). The β -laser has demonstrated thermal noise limited performance at the 10^{-15} fractional frequency level [4]. The optical beat (Fig. 2(a)) is limited by the thermal noise of the β -laser out to 10 Hz, where it becomes limited by the noise floor of the detector; however, discrete features are visible above this noise floor. Pairs of narrow noise peaks are visible near both 22 and 30 Hz. Additionally, noise peaks are consistently measured at 24 and 60 Hz. The 60 Hz peak is dominated by detector noise and the 24 Hz peak is visible in previous beat measurements between two β -lasers [4].

The spectroscopy sequences are performed such that the measured \mathbb{P} is sensitive to frequency noise from the α -laser.

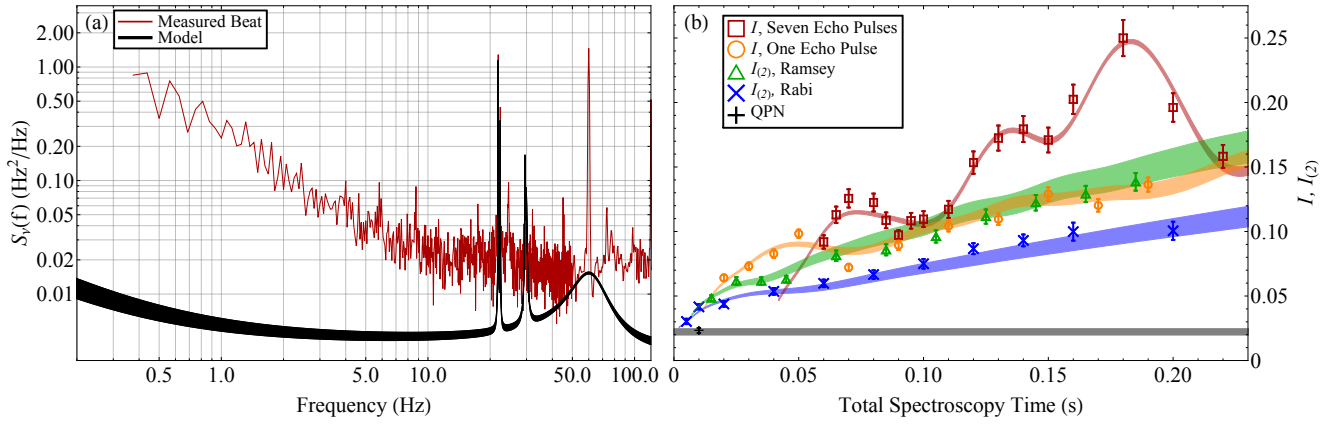


FIG. 2. (Color online) (a) The measured $S_\nu(f)$ of a beat between the α - and β -lasers is plotted in red. A model $S_\nu(f)$ for the α -laser is plotted as a black band (see text). (b) Measured values of I or $I_{(2)}$ are plotted as a function of total spectroscopy time for the spectroscopy sequences shown in Fig. 1. Colored bands represent calculated values of I or $I_{(2)}$ using the model $S_\nu(f)$ in (a) with QPN added in quadrature. A gray band indicates the mean calculated QPN for all experimental data. The black cross represents a measurement of the QPN (see text).

For Rabi spectroscopy, we detune the α -laser from resonance by the half width at half maximum (HWHM) of the Rabi line shape and subject the atoms to a π -pulse. For Ramsey spectroscopy, we tune the laser exactly on resonance and subject the atoms to two $\pi/2$ pulses separated in time. We shift the phase of the final $\pi/2$ pulse by $\pi/2$ radians relative to the initial $\pi/2$ pulse, which is equivalent to detuning by the HWHM of the central Ramsey fringe in the absence of phase shifts. The echo pulse sequences add to the Ramsey sequence a number of π -pulses introduced such that the free evolution times between laser pulses are all equal. The echo pulse sequences act as a bandpass filter peaked at $(n + 1)/(2\tau)$ Hz, where n is the number of echo pulses and τ is the total spectroscopy time. One can intuitively understand this behavior from the sensitivity functions in Fig. 1(d), which are periodic at this frequency. The Fourier transforms of $r(t)$ explicitly demonstrate this frequency sensitivity in Fig. 1(e). To prevent the accumulation of pulse area errors, we switch the phase of the laser between adjacent echo pulses by π rad.

We use 80 consecutive measurements of the atomic populations to estimate the raw standard(pair) deviation and its statistical uncertainty. The standard(pair) deviation is divided by the measured contrast to give $I(I_{(2)})$. The contrast is determined by a fit to the measured line shape as a function of detuning for Rabi spectroscopy or a fit to the measured oscillations of population when the phase of the final spectroscopy pulse is scanned for Ramsey and echo pulse spectroscopy. Fig. 2(b) shows measured values of I or $I_{(2)}$ for different spectroscopy sequences as a function of total spectroscopy time. Each data point represents a weighted mean of at least four measurements and the error bars are estimated from the variance of the weighted mean. Different spectroscopy times are applied in a random order to avoid systematic drifts. Each data point consists of measurements separated by several hours to insure consistency of the data.

We create a model $S_\nu(f)$ for the α -laser so that the calcu-

lated I and $I_{(2)}$ are consistent with experimentally measured values. The model $S_\nu(f)$, plotted in Fig. 2(a), accounts for a finite range of magnitudes for 1/f and white frequency noise which are necessary to simultaneously fit both the Rabi and Ramsey spectroscopy data. Due to its insensitivity to white and 1/f noise at the inferred magnitudes, the 7-echo pulse data is used to determine discrete noise contributions to the model $S_\nu(f)$. Two peaks are dominant in the 7-echo pulse data centered at 0.135 and 0.180 s of total spectroscopy time corresponding to noise components near 30 and 22 Hz respectively, consistent with the optical beat experiment. The noise at 30 Hz originates from alternating current motors and 22 Hz is approximately an acoustic resonance frequency of the lab.

The functional form of the model $S_\nu(f)$ is

$$S_\nu(f) = h_{\text{white}} + \frac{h_{\text{thermal}}}{f} + \sum_{i=1}^N \frac{h_i}{1 + \left(\frac{f-f_i}{\Gamma_i/2}\right)^2}, \quad (7)$$

where h_i , f_i , and Γ_i are the height, frequency, and full width at half maximum (FWHM) for the i th noise resonance. The parameters for these resonances are given in [21]. We determine h_{thermal} to be $1.5(4) \times 10^{-3}$ Hz², consistent with the predicted thermal noise of the cavity [26], and h_{white} to be $3.3(3) \times 10^{-3}$ Hz²/Hz. The widths and frequencies of the Lorentzian functions included in the model $S_\nu(f)$ are chosen to be consistent with features measured in the optical beat and the magnitudes are determined by the measured deviation of \mathbb{P} . A broad noise peak was also necessary in our model $S_\nu(f)$ to account for acoustic noise resonances between 40 and 80 Hz. This noise creates a small broad increase in I between 60 ms and 90 ms of total spectroscopy time for the 7-echo pulse data and was previously observed in a beat with the β -laser before a large acoustic shielding box was installed around the optics and vacuum chamber of the α -laser. Although an exact relationship between $S_\nu(f)$ and a FWHM linewidth has been

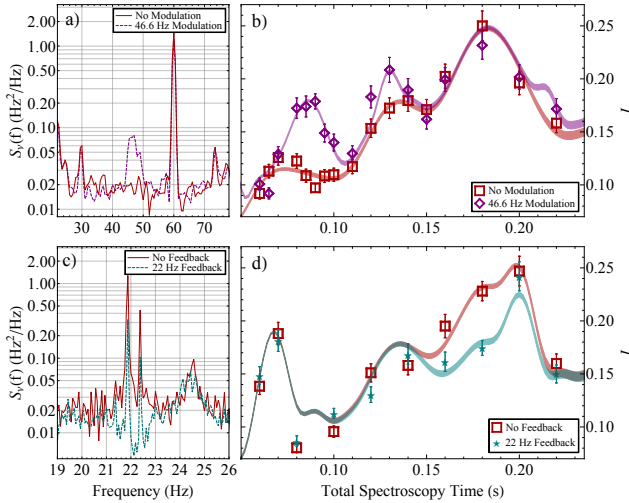


FIG. 3. (Color online) (a) Measured $S_{\nu}(f)$ of an optical beat between the α - and β -lasers and (b) measured and calculated values of I for a 7-echo pulse sequence with and without external modulation at 46.6 Hz. (c) Measured $S_{\nu}(f)$ of an optical beat between the α - and β -lasers and (d) measured and calculated values of I for a 7-echo pulse sequence with and without feedback cancellation of noise resonances near 22 Hz. (d) also demonstrates the appearance of 60 Hz noise due to a malfunctioning signal generator that increases the measured values of I at 0.06 and 0.2 s of total spectroscopy time.

established [29], an analytic expression for the linewidth does not exist in the presence of 1/f frequency noise. Here, the observed linewidth depends on the measurement time [30]. By properly accounting for a finite measurement time, we numerically calculate the minimum observable linewidth of the α -laser to be 26(4) mHz at 698 nm, dominated by the 1/f component of our model $S_{\nu}(f)$ [21].

For each data point, the QPN is calculated for the measured number of atoms and the mean excitation fraction. The mean QPN for each spectroscopy condition is calculated and added in quadrature with the calculated values of I and $I_{(2)}$ to more accurately represent the experimental data. These quantities are plotted as colored bands in Fig. 2(b) where the upper(lower) edge of the band corresponds to the upper(lower) edge of the model $S_{\nu}(f)$. The mean and standard deviation of all calculated QPN values are represented in Fig. 2(b) as a gray band. The QPN is experimentally measured by the standard deviation of repeated measurements of \mathbb{P} following a 5 ms, resonant, $\pi/2$ pulse. The measured and calculated QPN are consistent.

To further test our working model we intentionally add noise to the α -laser. White noise is passed through a bandpass filter at 46.6 Hz with 2 Hz bandwidth and used to frequency modulate the α -laser with an acoustic optical modulator (AOM). Fig. 3(a) demonstrates the effect of the modulation on the optical beat between the α - and β -lasers. By adding noise at 46.6 and 93.2 Hz into our model $S_{\nu}(f)$, corresponding to the 1st and 2nd order contributions of the modulation, we are able to fully account for the measured values

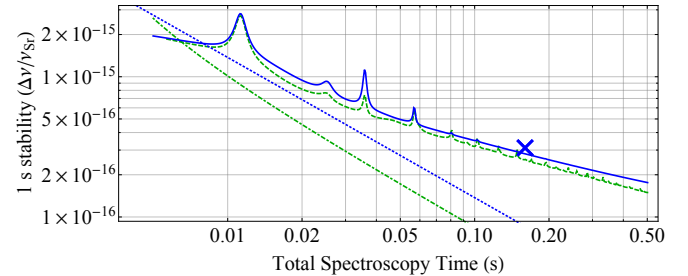


FIG. 4. (Color online) The solid blue (dashed green) line represents the 1 s stability limit for an optical clock due to the Dick effect using Rabi (Ramsey) spectroscopy as a function of total spectroscopy time. The blue dotted (green dot-dashed) line represents the QPN stability limit at 1 s for Rabi (Ramsey) spectroscopy assuming a collection of 2000 uncorrelated atoms. Ramsey spectroscopy assumes 2.5 ms $\pi/2$ pulses. The blue “x” denotes the implied single clock 1 s stability from [28].

of I with modulation. Calculated and measured values of I are shown in Fig. 3(b) for 7-echo pulse spectroscopy with and without 46.6 Hz modulation added to the α -laser.

In addition to using the optical beat to confirm the validity of our atomic measurements, we are also able to harness the information contained within the beat to reduce discrete noise features on the α -laser. We filter the beat with a bandpass centered at 22 Hz with sub-hertz bandwidth. This signal is inverted and fed back onto the α -laser with an AOM. We can observe the effect of the 22 Hz modulation on the beat itself (Fig. 3(c)). The effectiveness of this technique is demonstrated by a reduction in the measured I between 0.15 and 0.20 s of total spectroscopy time when feedback is active (Fig. 3(d)). In order to reproduce the measured values of I with feedback, the magnitude of the 22 Hz features needed to be reduced by 60% in the model $S_{\nu}(f)$ compared to the condition without feedback modulation.

Having developed an accurate model for the α -laser's $S_{\nu}(f)$, we can predict the stability this laser can achieve when used in an optical atomic clock. Here, the laser's frequency is slaved to the $|g\rangle$ to $|e\rangle$ transition in ^{87}Sr by periodic interrogation of this transition. The stability of this frequency standard is limited by the Dick effect [15–17], whereby the periodic nature of interrogation creates sensitivity to laser noise at harmonics of $1/T_c$. In Fig. 4, we plot the one second stability limit due to the Dick effect for Rabi and Ramsey spectroscopy as a function of total spectroscopy time, τ , using the lower limit of the model $S_{\nu}(f)$. We assume a typical T_c of 857.5 ms plus spectroscopy time. We find that for Rabi spectroscopy with 160 ms interrogation time, the Dick effect limits the stability of a clock using the α -laser to $2.8 \times 10^{-16}/\sqrt{\tau}$ in fractional frequency units. For a comparison of two uncorrelated clocks, one operating with 1000 atoms and one operating with 2000 atoms, we predict a stability of $4.6 \times 10^{-16}/\sqrt{\tau}$ which is within 5% of the achieved stability reported in [28].

We thank R. Ozeri for stimulating discussions on dynamical decoupling and J. K. Thompson and Z. Chen for parallel work

and discussions on the treatment of oscillator phase noise in the Bloch vector picture [31]. We acknowledge funding support for this work by DARPA QuASAR, NIST, and NSF. M. B. acknowledges support from NDSEG.

[1] J. Rutman, Proc. of the IEEE, **66**, 1048 (1978).

[2] B. C. Young, F. C. Cruz, W. M. Itano, and J. C. Bergquist, Phys. Rev. Lett. **82**, 3799 (1999).

[3] H. Stoehr, F. Mensing, J. Helmcke, and U. Sterr, Opt. Lett. **31**, 736 (2006).

[4] A. D. Ludlow *et al.*, Opt. Lett. **32**, 641 (2007).

[5] J. Alnis, A. Matveev, N. Kolachevsky, Th. Udem, and T. W. Hänsch, Phys. Rev. A **77**, 053809 (2008).

[6] P. Dubé, A. A. Madej, J. E. Bernard, L. Marmet, A. D. Shiner, Appl. Phys. B **95**, 43 (2009).

[7] Y. Y. Jiang *et al.*, Nat. Photonics **5**, 158 (2011).

[8] Y. N. Zhao, J. Zhang, A Stejskal, T. Liu, V. Elman, Z. H. Lu, and L. J. Wang, Opt. Express **17**, 8970 (2009).

[9] T. Kessler *et al.*, Nat. Photonics **6**, 687 (2012).

[10] L. S. Cutler, and C. L. Searle, Proc. of the IEEE, **54**, 136 (1966).

[11] L. Viola, E. Knill, and S. Lloyd, Phys. Rev. Lett. **82**, 2417 (1999).

[12] M. J. Biercuk, H. Uys, A. P. VanDevender, N Shiga, W. M. Itano, and J. J. Bollinger, Nature **458**, 996 (2009).

[13] S. Kotler, N. Akerman, Y. Glickman, A. Keselman, and R. Ozeri, Nature **473**, 61 (2011).

[14] J. Bylander *et al.*, Nat. Physics **7**, 565 (2011).

[15] G. J. Dick, Proc. 19th PTTI Applications and Planning Mtg., 133 (1987).

[16] G. Santarelli *et al.*, IEEE Trans. Ultrason., Ferroelect., Freq. Contr. **45**, 887 (1998).

[17] A. Quessada, R. P. Kovacich, I. Courtillot, A. Clairon, G. Santarelli, and P. Lemonde, J. Opt. B: Quantum Semiclass. Opt. **5**, S150 (2003).

[18] We note that our treatment is consistent with that in [31].

[19] D. Meiser, J. Ye, D. R. Carlson, and M. J. Holland, Phys. Rev. Lett. **102**, 163601 (2009).

[20] M. J. Martin, D. Meiser, J. W. Thomsen, J. Ye, and M. J. Holland, Phys. Rev. A **84**, 063813 (2011).

[21] See supplemental material.

[22] D. W. Allan, Proc. of the IEEE, **54**, 221 (1966).

[23] M. Bishof *et al.*, Phys. Rev. A **84**, 052716 (2011).

[24] G. K. Campbell *et al.*, Metrologia **45**, 539 (2008).

[25] J. Ye, H. J. Kimble, and H. Katori, Science **320**, 1734 (2008).

[26] M. D. Swallows *et al.*, IEEE Trans. Ultrason., Ferroelect., Freq. Contr. **59**, 416 (2012).

[27] M. J. Martin, M. Bishof, M. D. Swallows, X. Zhang, C. Benko, J. von-Stecher, A. V. Gorshkov, A. M. Rey, and J. Ye, arXiv:1212.6291.

[28] T. L. Nicholson *et al.*, Phys. Rev. Lett. **109**, 230801 (2012).

[29] D. S. Elliott, R. Roy, and S. J. Smith, Phys. Rev. A **26**, 12 (1982).

[30] G. Di Domenico, S. Schilt, and P. Thomann, Appl. Opt. **49**, 4801 (2010).

[31] Z. Chen, J. G. Bohnet, J. M. Weiner, and J. K. Thompson, Phys. Rev. A **86**, 032313 (2012).

**Supplementary online material to the manuscript:
“An optical spectrum analyzer with quantum limited noise floor”**

M. Bishof, X. Zhang, M. J. Martin, and Jun Ye

*JILA, National Institute of Standards and Technology and University of Colorado,
Department of Physics, University of Colorado, Boulder, CO 80309, USA.*

DERIVATION OF THE DETUNING-DRESSED BASIS HAMILTONIAN

We start with the Schrödinger equation for a two-level atom driven by a laser field with a frequency that can vary in time. This is most simply treated using the instantaneous phase of the laser, $\phi_L(t) = \int_0^t \omega_L(t') dt'$, where $\omega_L(t)$ is the instantaneous frequency of the laser. For a general state $|\psi\rangle = c_g(t)|g\rangle + c_e(t)|e\rangle$, we get the coupled differential equations:

$$\begin{aligned} i\dot{c}_e(t) &= \frac{\omega_a}{2}c_e(t) - \frac{\Omega(t)}{2}(e^{i\phi_L(t)} + e^{-i\phi_L(t)})c_g(t), \\ i\dot{c}_g(t) &= -\frac{\omega_a}{2}c_g(t) - \frac{\Omega(t)}{2}(e^{i\phi_L(t)} + e^{-i\phi_L(t)})c_e(t). \end{aligned} \quad (\text{S1})$$

Here, $\Omega(t)$ is the Rabi frequency and ω_a is the frequency of the $|g\rangle$ to $|e\rangle$ transition.

To simplify the solutions to these equations, we substitute the complex state coefficients with

$$\tilde{c}_e(t) \equiv e^{i\omega_a t/2}c_e(t) \quad \text{and} \quad \tilde{c}_g(t) \equiv e^{-i\omega_a t/2}c_g(t). \quad (\text{S2})$$

Using this substitution, (S1) becomes

$$\begin{aligned} &\frac{\omega_a}{2}e^{-i\omega_a t/2}\tilde{c}_e(t) + ie^{-i\omega_a t/2}\dot{\tilde{c}}_e(t) \\ &= \frac{\omega_a}{2}e^{-i\omega_a t/2}\tilde{c}_e(t) - \frac{\Omega(t)}{2}(e^{i\phi(t)} + e^{-i\phi(t)})e^{i\omega_a t/2}\tilde{c}_g(t), \\ &-\frac{\omega_a}{2}e^{i\omega_a t/2}\tilde{c}_g(t) + ie^{i\omega_a t/2}\dot{\tilde{c}}_g(t) \\ &= -\frac{\omega_a}{2}e^{i\omega_a t/2}\tilde{c}_g(t) - \frac{\Omega(t)}{2}(e^{i\phi(t)} + e^{-i\phi(t)})e^{-i\omega_a t/2}\tilde{c}_e(t). \end{aligned} \quad (\text{S3})$$

We can cancel an overall phase factor of $e^{-(+/-)i\omega_a t/2}$ from the top(bottom) equation in (S3) and simplify to get

$$\begin{aligned} i\dot{\tilde{c}}_e(t) &= -\frac{\Omega(t)}{2}(e^{i(\phi_L(t)+\omega_a t)} + e^{-i(\phi_L(t)-\omega_a t)})\tilde{c}_g(t), \\ i\dot{\tilde{c}}_g(t) &= -\frac{\Omega(t)}{2}(e^{i(\phi_L(t)-\omega_a t)} + e^{-(i\phi_L(t)+\omega_a t)})\tilde{c}_e(t). \end{aligned} \quad (\text{S4})$$

In order to proceed, we assume that the instantaneous laser frequency is the sum of a constant frequency and a small noise term that varies in time, $\omega_L(t) = \omega_{L_0} + \delta\omega(t)$. Then we can write the instantaneous phase of the laser as $\phi_L(t) = \omega_{L_0}t + \int_0^t \delta\omega(t') dt' \equiv \omega_{L_0}t + \delta\phi(t)$. Substituting this into (S4), we

get:

$$i\dot{\tilde{c}}_e(t) = -\frac{\Omega(t)}{2} \times (e^{i(\omega_{L_0}t+\delta\phi(t)+\omega_a t)} + e^{-i(\omega_{L_0}t+\delta\phi(t)-\omega_a t)})\tilde{c}_g(t),$$

$$i\dot{\tilde{c}}_g(t) = -\frac{\Omega(t)}{2} \times (e^{i(\omega_{L_0}t+\delta\phi(t)-\omega_a t)} + e^{-i(\omega_{L_0}t+\delta\phi(t)+\omega_a t)})\tilde{c}_e(t). \quad (\text{S5})$$

Since, $\delta\phi(t)$ is assumed to be small, we can make the usual rotating wave approximation where we neglect terms that rotate at the sum of ω_{L_0} and ω_a . The resulting equations are

$$\begin{aligned} i\dot{\tilde{c}}_e(t) &= -\frac{\Omega(t)}{2}e^{-i(\bar{\Delta}t+\delta\phi(t))}\tilde{c}_g(t), \\ i\dot{\tilde{c}}_g(t) &= -\frac{\Omega(t)}{2}e^{i(\bar{\Delta}t+\delta\phi(t))}\tilde{c}_e(t). \end{aligned} \quad (\text{S6})$$

where, $\bar{\Delta} \equiv \omega_{L_0} - \omega_a$.

Another basis change is necessary before arriving at the final result, so we express (S6) in terms of new state coefficients defined as

$$b_e(t) \equiv e^{-i\bar{\Delta}t/2}\tilde{c}_e(t) \quad \text{and} \quad b_g(t) \equiv e^{i\bar{\Delta}t/2}\tilde{c}_g(t). \quad (\text{S7})$$

After canceling overall phase factors we get the following differential equations.

$$\begin{aligned} i\dot{b}_e(t) &= -\frac{\Omega(t)}{2}e^{-i\delta\phi(t)}b_g(t) + \frac{\bar{\Delta}}{2}b_e(t), \\ i\dot{b}_g(t) &= -\frac{\Omega(t)}{2}e^{i\delta\phi(t)}b_e(t) - \frac{\bar{\Delta}}{2}b_g(t). \end{aligned} \quad (\text{S8})$$

This gives that the Hamiltonian in this basis is

$$\frac{\hat{H}}{\hbar} = -\frac{\Omega(t)}{2} \begin{pmatrix} 0 & e^{i\delta\phi(t)} \\ e^{-i\delta\phi(t)} & 0 \end{pmatrix} - \frac{\bar{\Delta}}{2}\hat{\sigma}_z, \quad (\text{S9})$$

where $\hat{\sigma}_z$ is a pauli spin matrix.

DERIVATION OF VARIANCE

Here we derive the variance of \mathbb{P} , starting with equation (3) in the main text. We assume that all measurements are made near $\mathbb{P} = 0$ so it will be sufficient to calculate the quantity

$$\langle \mathbb{P}^2 \rangle = \left\langle \int_{-\infty}^{\infty} \int_{-\infty}^{\infty} dt_1 dt_2 \Delta(t_1) r(t_1) \Delta(t_2) r(t_2) \right\rangle. \quad (\text{S10})$$

This expression can be simplified using the definition of the convolution operation along with the definition of the auto-correlation function,

$$\mathcal{R}_f(t_1 - t_2) = \langle f(t_1) f^*(t_2) \rangle, \quad (\text{S11})$$

where R_f is the autocorrelation function of f . Then, equation (S10) simplifies to

$$\langle \mathbb{P}^2 \rangle = \int_{-\infty}^{\infty} dt (\mathcal{R}_\Delta \star r)(t) r(t), \quad (\text{S12})$$

where “ \star ” represents convolution. Since an oscillator’s noise properties are typically characterized in frequency space via a power spectral density, we employ Parseval’s theorem, which relates the integral of two complex valued functions $x(t)$ and $y(t)$ of time to the integral of their Fourier transforms $X(f)$ and $Y(f)$ as follows

$$\int_{-\infty}^{\infty} dt x(t) y^*(t) = \int_{-\infty}^{\infty} df X(f) Y^*(f). \quad (\text{S13})$$

Here, f^* denotes the complex conjugate of f . Since $r(t)$ is real valued, we get that

$$\int_{-\infty}^{\infty} dt (\mathcal{R}_\Delta \star r)(t) r(t) = \int_{-\infty}^{\infty} df \mathcal{F}[(\mathcal{R}_\Delta \star r)](f) R^*(f), \quad (\text{S14})$$

where \mathcal{F} is the fourier transform operation and $R(f)$ is the Fourier transform of $r(t)$. The convolution theorem states that the Fourier transform of a convolution of two functions is equal to the product of the Fourier transforms of the two functions. Additionally, the Wiener-Khinchin theorem states that the power spectral density (PSD) of a function, f , is equal to the Fourier transform of the autocorrelation function of f . Thus, we get that

$$\langle \mathbb{P}^2 \rangle = \int_{-\infty}^{\infty} df S_\Delta(f) |R(f)|^2, \quad (\text{S15})$$

where $S_\Delta(f)$ is the double sided PSD of the laser in units of $(\text{rad/s})^2/\text{Hz}$. We can express the variance in terms of the more commonly used single sided PSD with units of Hz^2/Hz to obtain the final result

$$I^2 = \langle \mathbb{P}^2 \rangle = (2\pi)^2 \int_0^{\infty} df S_\nu(f) |R(f)|^2. \quad (\text{S16})$$

Here, we have use the relationship, $S_\Delta(f) = (2\pi)^2 S_\nu(f)/2$ for $f \geq 0$.

DERIVATION OF THE TWO SAMPLE ALLAN VARIANCE

We begin with the definition for the two-sample Allan variance:

$$I_{(2)}^2 \equiv \frac{1}{2} \langle (\mathbb{P}_{i+1} - \mathbb{P}_i)^2 \rangle, \quad (\text{S17})$$

Then the expression for the two-sample Allan variance is completely analogous to (S10) under the substitution

$$r(t) \rightarrow r_{(2)}(t) \equiv r(t) - r(t - T_c). \quad (\text{S18})$$

Since the Fourier transform operation is linear and a shift in time of T_c simply adds a phase factor of $e^{-2\pi i T_c f}$ to the Fourier transform of $r(t)$, we get that

$$\begin{aligned} \mathcal{F}[r_{(2)}(t)] &= \mathcal{F}[r(t)] - \mathcal{F}[r(t - T_c)] \\ &= 2ie^{-\pi i T_c f} \sin(\pi T_c f) R(f). \end{aligned} \quad (\text{S19})$$

This shows that $I_{(2)}^2$ can be expressed in terms of $R(f)$ as

$$I_{(2)}^2 = (2\pi)^2 \int_0^{\infty} df S_\nu(f) 2 \sin^2(\pi f T_c) |R(f)|^2. \quad (\text{S20})$$

TABLE OF PARAMETERS FOR MODEL PSD FEATURES

Index	f_i (Hz)	h_i (Hz 2 /Hz)	Γ_i (Hz)
1	21.87	1.2 [1]	0.03
2	22.39	0.6 [1]	0.03
3	29.45	0.15	0.1
4	29.90	0.08	0.4
5	60	0.012	27
Added Noise			
6	46.6	0.07	2
7	93.2	0.25	2

CALCULATION OF THE LASER LINENWIDTH

To calculate the linewidth of the α -laser, we express the autocorrelation function for the laser’s electric field, $R_E(\tau)$, in terms of the frequency noise PSD, $S_\nu(f)$, and take the Fourier transform of $R_E(\tau)$ to get the laser line shape function [2, 3]. We consider an electric field of the form

$$E(t) = E_0 e^{i(2\pi\nu_{L_0} t + \delta\phi(t))}, \quad (\text{S21})$$

where $\nu_{L_0} \equiv \omega_{L_0}/2\pi$. Then the $R_E(\tau)$ can be expressed in terms of $S_\nu(f)$ as follows: [3]

$$R_E(\tau) = E_0^2 e^{i2\pi\nu_{L_0} \tau} e^{-2 \int_0^{\infty} S_\nu(f) \frac{\sin^2(\pi f \tau)}{f^2} df}. \quad (\text{S22})$$

Since the model $S_\nu(f)$ that we deduce from our measurements contains a component proportional to $1/f$, the integral in the exponent diverges and we must take into account the

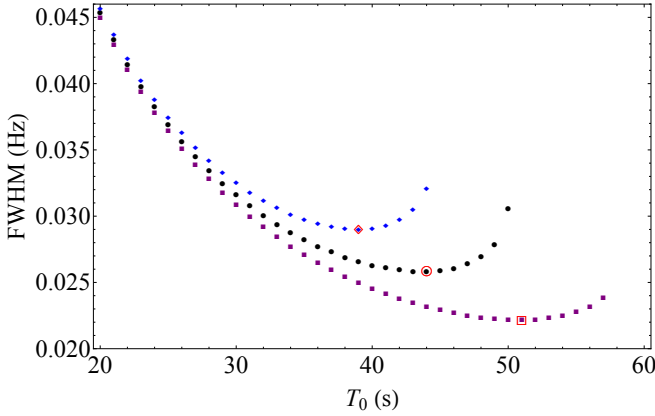


FIG. S1. (Color online) The numerically calculated FWHM of the α -laser as a function of observation time. Black circles represent calculations using the model $S_\nu(f)$ that is quoted in the main text, excluding narrow resonance features that do not contribute to the FWHM. Blue diamonds(purple squares) represent calculations using the upper(lower) limit quoted for $S_\nu(f)$. The minimum value for each condition is outlined in red. These values determine the minimum observable linewidth for the α -laser: 26(4) mHz.

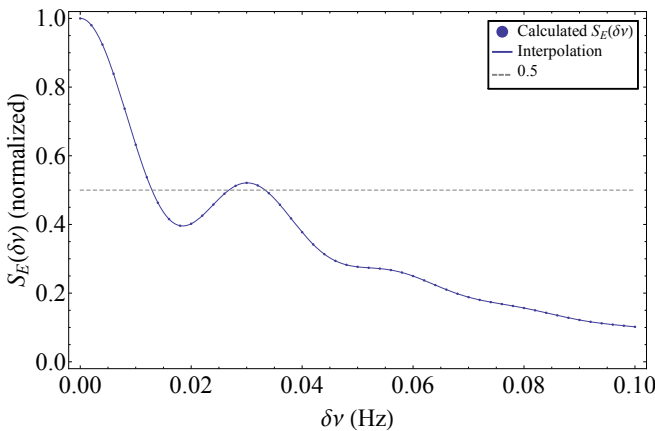


FIG. S2. (Color online) The calculated line shape, $S_E(\delta\nu)$, using $h_{\text{white}} = 0.0033 \text{ Hz}^2/\text{Hz}$, $h_{\text{thermal}} = 0.0015 \text{ Hz}^2$, and $T_0 = 44 \text{ s}$. This measurement time corresponds to the minimum FWHM of $S_E(\nu)$ for these values of $S_\nu(f)$. A dashed gray line signifies the half maximum to guide the eye.

measurement time over which the laser is observed. A measurement lasting T_0 s is insensitive to frequency noise below $1/T_0$ Hz. This dictates that the lower bound of the integral in Eqn. (S22) should be set to $1/T_0$, thereby making the integral finite. The finite observation time also scales $R_E(\tau)$ by a triangle bump function since the measurement is windowed by a

flat rectangle function between $t = 0$ and $t = T_0$. Therefore, the line shape observed over a finite time T_0 will depart from a simple Fourier transform of $R_E(\tau)$ and take the form

$$S_E(\nu) = 2 \int_{-T_0}^{T_0} \left(1 - \frac{|\tau|}{T_0}\right) e^{-i2\pi\nu\tau} R_E(\tau) d\tau, \quad (\text{S23})$$

which can be simplified to

$$S_E(\delta\nu) = 4E_0^2 \int_0^{T_0} \left(1 - \frac{|\tau|}{T_0}\right) \cos(2\pi\delta\nu\tau) \times e^{-2 \int_{1/T_0}^{\infty} S_\nu(f) \frac{\sin^2(\pi f\tau)}{f^2} df} d\tau, \quad (\text{S24})$$

where $\delta\nu \equiv \nu - \nu_{L_0}$.

To calculate the minimum observable FWHM, we compute the FWHM of $S_E(\delta\nu)$ as a function of T_0 for the model $S_\nu(f)$ quoted in the main text and its upper and lower bounds. The three conditions lead to three minimum linewidths, observable at three different measurement times (Fig. S1) and determine the minimum observable linewidth of the α -laser to be 26(4) mHz. The calculated line shape, $S_E(\delta\nu)$, using $h_{\text{white}} = 0.0033 \text{ Hz}^2/\text{Hz}$ and $h_{\text{thermal}} = 0.0015 \text{ Hz}^2$ is plotted in Fig. S2 for the measurement time that give the minimum FWHM, $T_0 = 44 \text{ s}$. In practice we only include the white, 1/f, and broad acoustic resonance #5 contributions to $S_\nu(f)$ for this calculation because the narrow peaks increase computation time and we have confirmed that these peaks do not significantly affect the calculated FWHM (< 0.1% effect for tested times). For $T_0 < 30 \text{ s}$, the FWHM is dominated by the Fourier limit of the triangular windowing function (FWHM = $0.8859/T_0$ for $S_\nu(f) = 0$) with a small contribution from white noise ($h_{\text{white}} = 0.0033(3) \text{ Hz}^2/\text{Hz}$ leads to a Lorentzian linewidth of 10(1) mHz). Between $T_0 \cong 40 \text{ s}$ and $T_0 \cong 60 \text{ s}$, the line shape can cross 50% of its peak value multiple times: a result of side bumps in the line shape arising from the windowing function and from the increasing contribution of 1/f noise as T_0 increases. We always calculate the FWHM from the lowest frequency half maximum crossing.

[1] We note that an overall 17% reduction in the strength of these features was necessary for the data plotted in figure 3(d), corresponding to daily variation in the acoustic environment. A further 60% reduction was necessary for the condition with feedback active (see main text).
[2] D. S. Elliott, R. Roy, and S. J. Smith, Phys. Rev. A **26**, 12 (1982).
[3] G. Di Domenico, S. Schilt, and P. Thomann, Appl. Opt. **49**, 4801 (2010).